Colloquia: FATA 2019

Precise timing with the PICOSEC-Micromegas detector

D. Sampsonidis(4)(*), J. Bortfeldt(2)(**), F. Brunbauer(2), C. David(2),
D. Desforge(1), G. Fanourakis(5), J. Franchi(2), M. Gallinaro(7),
F. García(11), I. Giomataris(1), T. Gustavsson(9), C. Guyot(1),
F. J. Iguaz(1)(***), M. Kebbiri(1), K. Kordas(4), C. Lampoudis(4), P. Legou(1),
J. Liu(3), M. Lupberger(2)(✱), O. Maillard(1), V. Maniatis(4), I. Manthos(4),
H. Müller(2), E. Oliveri(2), T. Papaevangelou(1), K. Paraschou(4),
M. Pomorski(10), F. Resnati(2), L. Ropelewski(2), T. Schneider(2),
P. Schwemling(1), E. Scorsone(10), L. Sohl(1), M. Van Stenis(2),
P. Thuiner(2), Y. Tsipolitis(6), S. E. Tzamarias(4), R. Veenhof(8)(✱✱),
X. Wang(3), S. White(2)(✱✱✱), Z. Zhang(3) and Y. Zhou(3)

(1) *IRFU, CEA, Université Paris-Saclay - F-91191 Gif-sur-Yvette, France*

(2) *European Organization for Nuclear Research (CERN) - CH-1211 Geneve 23, Switzerland*

(3) *State Key Laboratory of Particle Detection and Electronics, University of Science and Technology of China - Hefei 230026, China*

(4) *Department of Physics, Aristotle University of Thessaloniki - Thessaloniki, Greece*

(5) *Institute of Nuclear and Particle Physics, NCSR Demokritos - 15341 Agia Paraskevi, Attiki, Greece*

(6) *National Technical University of Athens - Athens, Greece*

(7) *Laboratório de Instrumentacão e Física Experimental de Partículas - Lisbon, Portugal*

(8) *RD51 Collaboration, European Organization for Nuclear Research (CERN) - CH-1211 Geneve 23, Switzerland*

(9) *LIDYL, CEA-Saclay, CNRS, Université Paris-Saclay - F-91191 Gif-sur-Yvette, France*

(10) *CEA-LIST, Diamond Sensors Laboratory, CEA-Saclay - F-91191 Gif-sur-Yvette, France*

(11) *Helsinki Institute of Physics, University of Helsinki - 00014 Helsinki, Finland*

(*) Corresponding author. E-mail: Dimitrios.Sampsonidis@cern.ch
(**) Now at Ludwig-Maximilians-University Munich, Germany.
(***) Now at Synchrotron Soleil, BP 48, Saint-Aubin, 91192 Gif-sur-Yvette, France.
(✱) Now at Physikalisches Institut, Universität Bonn, Germany.
(✱✱) Also at National Research Nuclear University MEPhI, Kashirskoe Highway 31, Moscow, Russia, and Department of Physics, Uludag University, 16059 Bursa, Turkey.
(✱✱✱) Also at University of Virginia, USA.

Summary. — This work presents the concept of the PICOSEC-Micromegas detector to achieve a time resolution below 30 ps. PICOSEC consists of a two-stage Micromegas detector coupled to a Cherenkov radiator and equipped with a photocathode. The results from single-channel prototypes as well as the understanding of the detector in terms of detailed simulations and preliminary results from a multichannel prototype are presented.

1. – Introduction

The needs emerging from the future High-Energy Physics (HEP) experiments have stimulated interest in developing tracking detectors with timing capabilities at high particle rates. In the High Luminosity LHC, every single proton-proton bunch crossing will result in a high multiplicity ($\sim$140) of proton-proton interactions piling-up close to each other ($\sigma \sim 45\,\mathrm{mm}$). The association of the particles to the correct vertex can be mitigated by timing the arrival of the particles with a resolution of the order of 30 ps [1].

The RD51 PICOSEC-Micromegas Collaboration developed a detector [2] (hereafter named PICOSEC) based on a two-stage Micromegas technology with timing capability reaching below 25 ps [3]. A Micromegas chamber (fig. 1) is coupled to a Cherenkov radiator and a photocathode so that a passing relativistic charged particle produces photons in the radiator, which subsequently generates electrons in the photocathode. These photoelectrons (PEs from here on) enter the Micromegas [4] drift region, which is reduced to ($\sim$200 m) in order to minimize the possibility of ionizations by the passing particle, while the anode region has the typical size for Micromegas ($128\,\mu$m). The PEs are produced almost synchronously and, even with modest voltage differences ($\sim$400 V), they start preamplification avalanches (pre-avalanches from here on) early in the drift region with a small time jitter.
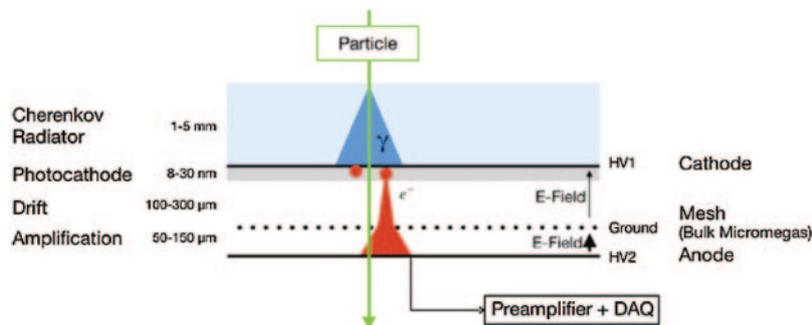

Fig. 1. – Layout of the PICOSEC-Micromegas detector. The passage of a charged particle through the Cherenkov radiator produces UV photons, which are then absorbed at the photocathode and partially converted into electrons. These electrons are subsequently preamplified and then amplified in the two high-field drift stages, and induce a signal which is measured between the anode and the mesh.
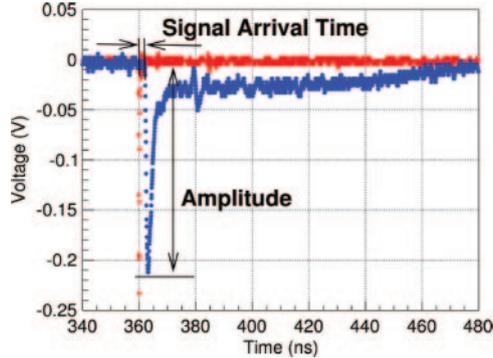
Fig. 2. – A pulse produced by the PICOSEC-Micromegas detector responding to 150 GeV muons (blue), recorded together with the timing reference (red) of a microchannel plate (MCP) signal.

Results presented here are produced with single or segmented anode (multi-pad) PICOSEC bulk Micromegas prototypes [5] where the Cherenkov radiator is a 3 mm thick MgF_2 layer, the photocathode is an 18 nm thick CsI film deposited on a 5.5 nm thick film of semitransparent Cr which provides conductivity to the cathode, the gas mixture is the COMPASS gas ($80\%Ne + 10\%C_2H_6 + 10\%CF_4$) at 1 bar.

2. – Response to single photoelectrons and to muons

Figure 2 shows the response of a single-channel PICOSEC detector (1 cm in diameter) to a 150 GeV muon (blue), digitized together with the timing reference signal (red) of a microchannel plate (MCP) by a 2.5 GHz oscilloscope every 50 ps. The PICOSEC signal contains a fast component with a 500 ps rise-time and a duration of order ns called the e-peak, produced by the fast drifting electrons, and a slower component generated by the slowly moving ion drift. The collected digitized waveforms were analysed offline to determine the e-peak start and end times, the e-peak charge and amplitude and the Signal Arrival Time (SAT), which is defined at 20% of the peak amplitude (*i.e.*, using the Constant Fraction Discrimination (CFD) technique). The SAT, as illustrated in fig. 2, is defined as the difference between the PICOSEC CF time and that of the reference detector. The SAT distribution was fit to the sum of two Gaussians, whose weighted RMS yielded the resolution.

Single PE data were collected at the IRAMIS facility at CEA-Saclay, using a pulsed laser beam. The laser beam was split with one part properly attenuated in order to provide single photon pulses on the PICOSEC, and the other part to illuminate a photodiode used as a time reference with a precision of 13 ps. The performance of the PICOSEC prototypes was also evaluated with 150 GeV muon beam data, collected at the SPS H4 beam line at CERN. In the muon test beam, MicroChannel Plates (MCP) provided the time reference with a precision of 4 ps, while scintillators provided the trigger. Three GEM detectors were used to track the incident muons, as described in [3]. In all data-taking setups mentioned in this contribution, the PICOSEC signal passed through a CIVIDEC preamplifier and was digitized by high-bandwidth fast digital oscilloscopes (2.5 GHz LeCroy, 20 Gs/s).

The time resolution improved with higher drift voltages, with a smaller dependence on the anode voltage. The best resolution for single PEs was found to be (76.0 ± 0.4) ps, at an anode/drift voltage of $+450\,V/-425\,V$, respectively. The SAT was also found (see
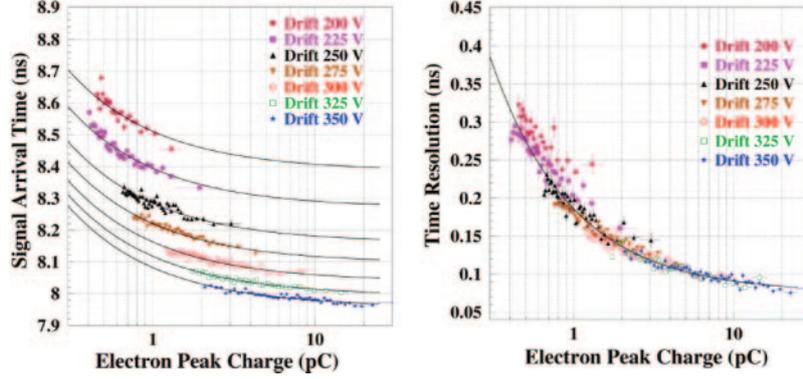
Fig. 3. – Mean SAT values (left) and time resolution (right) as a function of the e-peak charge, for single PE data, for a fixed anode voltage of $+525\,\mathrm{V}$ and drift voltages between -200 and $-350\,\mathrm{V}$.

fig. 3, left) to vary with the e-peak charge, with the same power law for all drift voltages, but shifted to lower levels for higher voltage settings. This shift reflects the increased electron drift velocity for higher drift voltages, but the dependence of the SAT on the e-peak charge is not evident. Since it was found that the pulse shape is identical for different e-peak charges, the use of the CFD technique should yield the same SAT for all pulses. Therefore, the observed SAT dependence on the e-peak charge must be caused by the physical mechanism generating the PICOSEC-Micromegas signal.

For muons (MIPs), the best resolution was $(24.0 \pm 0.3)\,\mathrm{ps}$, as fig. 4 shows, obtained with an anode/drift voltage of $+275\,\mathrm{V}/-475\,\mathrm{V}$, respectively. The inadequacy of a single Gaussian to determine the resolution indicates that not all pulses have the same resolution. It was found, in both the muon and the single PE data (see fig. 3, right), that the resolution improves as the e-peak charge increases, with the same dependence for all drift voltages.
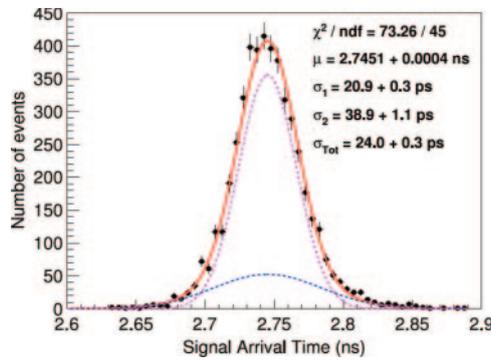

Fig. 4. – Muons generate multiple PEs and thus bigger signals with improved resolution. The distribution of e-peak charges generated by single PE is described well by a Polya function (a Gamma distribution). For muons the distribution is also a Polya, which results from the convolution of the single PE Polya and a Poisson describing the number of generated PEs. The mean number of PEs per muon is found to be 10.4 ± 0.4 for this nominal PICOSEC-Micromegas with a CsI photocathode.

3. – Simulation and modeling

A detailed simulation was performed based on Garfield++ [6] in order to understand the observed dependences of the PICOSEC timing characteristics on the e-peak charge. All the relevant processes starting from the emission of the PE from the cathode, up to the transmission of the preamplification avalanche electrons through the mesh to the anode region, were simulated. A 2.5 mV RMS uncorrelated electronic noise and the response of the electronics to the amplification avalanche was also included [7]. Assuming a linear response of the electronics, the simulation produces waveforms, which were digitized and treated exactly the same way as the experimental waveforms. By applying the same signal processing and analysis to the simulated events, the same dependence of the SAT and the timing resolution on the e-peak charge as in experimental data was found, as shown in fig. 3.

The agreement between simulation and data justifies the use of Garfield++ in investigating the microscopic variables that determine the observed signal characteristics. As described in detail in [7], it was found that there is a microscopic parameter with the same statistical properties as the SAT, in every bin of the e-peak charge: this is the average arrival time of the preamplification electrons into the amplification region, having just traversed the mesh. The statistical properties of the above time average are determined by the three phases of the signal formation: i) the PE drift until it causes the first ionization; ii) the evolution of preamplification avalanche; and iii) the passage of the preamplification electrons through the mesh. The transmission time through the mesh is found to be a constant. While the mean transmission time through the mesh is found to be independent of the e-peak charge, both the PE and preamplification avalanche mean transmission times increase linearly with their respective drift distance; but the pre-avalanche has a higher effective drift velocity than the primary PE ($154\,\mu$m/ns *vs.* $134\,\mu$m/ns, respectively, for a drift/anode voltage of $-425\,$V$/+450\,$V).

As the number of preamplification electrons determines the e-peak charge and this number depends exponentially on the length of the preamplification avalanche, this difference in drift velocities causes larger e-peak signals to arrive earlier than smaller ones. Furthermore, as found in the detailed Garfield++ simulation studies [6], the avalanche transmission time depends also, explicitly, logarithmically on the number of the preamplification electrons due to gains in time at each secondary electron production.

Both the above-mentioned effects result in avalanches with larger e-peak charges to arrive earlier than avalanches with smaller e-peak charges, with the same functional dependence as observed in the data. In these simulation studies it was also found that the spread of the PE transmission time increases with larger drift paths, while the spread of the preamplification avalanches transmission time is saturated at a constant value. Therefore, the sooner the primary PE ionizes for the first time, the better the timing resolution is (see fig. 5, right). Due to the correlation of the avalanche length with the number of electrons produced in the avalanche, the spread of the SAT is a decreasing function of the number of the preamplification electron as it is shown on the left plot of fig. 5.

In order to gain insight on the main physical mechanisms causing the findings mentioned above, a phenomenological model was built [8]. Motivated by the known fact in the literature that quenchers in the gas-mix increase the drift velocity, the model is based on a simple mechanism of time gain per inelastic interaction compared to an elastic interaction and it employs a statistical description of the avalanche evolution, taking into account all correlations between the various players. The model describes the dynam-
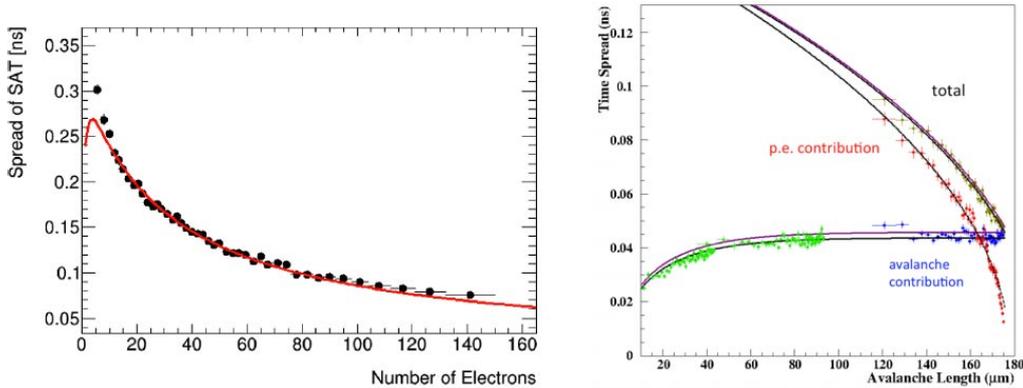
Fig. 5. – Left: the spread of the total transmission time *vs.* the number of electrons reaching the mesh. All results are from detailed Garfield++ simulations with anode and drift voltages of $+450\,\mathrm{V}$ and $-425\,\mathrm{V}$, respectively. The lines are not fits to the data but predictions of the model (see text). Right: spread of transmission times *vs.* preamplification avalanche length for i) the primary PE before it ionizes for the first time (red points); ii) the preamplification avalanche from its initiation till the mesh (blue points; green points correspond to avalanches which have not yet reached the mesh); and iii) the total transmission time from the creation of the primary PE to the arrival of the preamplification avalanche to the mesh (black points).

ical and statistical properties of the microscopic quantities determining the PICOSEC timing characteristics, in an excellent agreement with the detailed simulations (see lines in fig. 4). Since it uses complete PDFs in its equations, it does not only describe mean and RMS values, but full distributions as well. In parallel, it offers phenomenological explanations to the behavior of the microscopic variables (*e.g.*, the faster drifting of the pre-avalanche compared to the primary PE, the saturation of the time spread of the pre-avalanches electrons, etc.). The model can be used as a tool for fast and reliable predictions, provided the values of the model input-parameters (*e.g.*, drift velocities) are known. Having available sets of input parameter values for certain operational settings, empirical characterizations of the input parameters are derived, which can be used to provide input to the model for the whole region of operational settings covered by the above characterizations [8].

4. – Evaluation of the number of photoelectrons per muon track

In order to accurately estimate the mean number of PEs per muon for a given photocathode, a consistent and unbiased method was developed, which employs the e-peak charge distribution of PICOSEC signals responding to relativistic muons, in comparison with the distribution related to the response of the PICOSEC operating with the same parameters to single PE During the test beam and between muon runs, PICOSEC data were collected using a UV lamp adjusted to illuminate the detector with single photons. Figure 6 shows the e-peak charge distribution (black points) generated by 150 GeV muons and compared to the statistical prediction (red line) obtained from a maximum likelihood method. The inset plot shows the electron peak distribution generated by a signal from the UV lamp (black points) is fit by the single e-peak distribution (red line) plus a noise contribution (blue line). The settings are 275 V for the anode and 475 V for the drift voltages, in both cases. Statistical uncertainties are also shown.
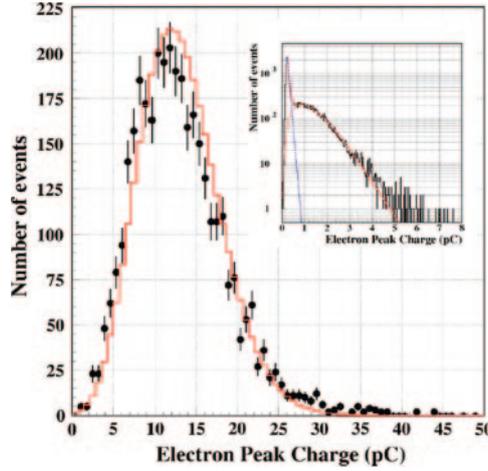
Fig. 6. – An example of the e-peak charge distribution (black points) generated by 150 GeV muons and compared to the statistical prediction (red line) obtained from a maximum likelihood method. Inset: the e-peak distribution generated by a signal from the UV lamp (black points) is fit by the single e-peak distribution (red line) plus a noise contribution (blue line). The settings are 275 V for the anode and 475 V for the drift voltages, in both cases. Statistical uncertainties are shown.

5. – Towards a robust and large scale PICOSEC detector

5˙1. *Robustness issues*. – After the heavy irradiation tests above though, it was seen with the microscope that the CsI photocathode was damaged. Ion back-flow can cause such damage, where ions created along with the electrons during the avalanche development are flowing back towards the cathode. Exposure of the photocathode to humidity in air, which can happen depending on the storage conditions, can also damage the photocathode and deteriorate its performance. A photocathode should also have a relatively high quantum efficiency, in order to get a reasonable number of PEs per passing muon. In fact, the time resolution is proportional to the inverse of the square root of the number of PEs; as seen earlier for the nominal device, the resolution for the single PE case is about $\sqrt{10.4}$ times bigger than the resolution for the muon case (76 ps *vs.* 24 ps, respectively). Various photocathodes were tested with these requirements in mind: from metallic (*e.g.*, Al), to CsI with thicker Cr layers than the nominal 5.5 nm, to diamond-like carbon (DLC) films. Preliminary results show that a 2.5 nm DLC film is promising, being robust against long storage periods and yielding around 3.7 PEs per muon, reaching a resolution down to 35–40 ps. More results can be found in [9].

5˙2. *Response of a multi-pad device to muon*. – On the way towards large-scale PICOSEC-Micromegas devices, a multi-pad prototype, with all other things like in the nominal detector configuration, has been constructed and tested in a muon beam. The anode is segmented in 5 mm side hexagonal pads and four of them were read out in a setup identical to the single-pad case but using two oscilloscopes. The response of each pad *vs.* the distance R of the track impact point from the pad center, was studied. The average e-peak charge will be smaller and smaller as the distance R increases, but the e-peak charge value incorporates the information about where is the Cherenkov cone centered compared to the pad center.
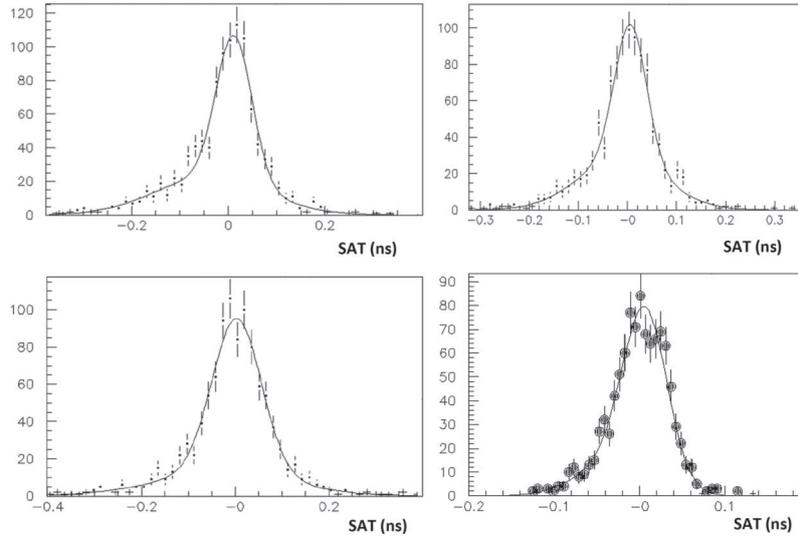
Fig. 7. – SAT distribution of each individual pad for tracks in the region between three pads, resulting in a timing resolution of 81 ps (top left), 70 ps (bottom left) and 86 ps (top right). SAT distribution combining the timing information from each pad and applying corrections (described in the text) resulting to 31 ps timing resolution (bottom right).

So, universal curves *vs.* e-peak charge should be observed for events with different R values. This was not the case due to some geometrical distortion of the chamber which resulted in a different response as a function of R and around each pads center. After correcting the observed SAT values for these effects, universal curves were obtained for the SAT and time resolution *vs.* e-peak charge; one pair of such curves for each pad.

Following the same analysis steps as for the single-pad prototype, each pad was found to have a preliminary time resolution of 25 ps, for tracks passing within 2 mm from its center. In the region between three pads the distance from each pad-center is maximum and each individual pad sees a smaller portion of the Cherenkov cone resulting to a smaller average e-peak charge; thus, each pad alone exhibits a resolution with preliminary values in the range 70–80 ps as shown in fig. 7 (left and top right). A naive combination of these individual-pad results would yield a time resolution around 45 ps for such tracks. But, since the expected SAT and time resolution of each event in each pad is known from the corresponding curves *vs.* the e-peak charge in each pad, a combined event-by-event measurement of the SAT can be obtained. The resolution of the SAT distribution is found to have the preliminary value of 30 ps (fig. 7, bottom right), close to the value obtained when the track goes through the center of each pad. Confidence to this result is obtained by observing that the pull distribution of the SAT values is a normal Gaussian, with a mean and sigma value consistent with zero and one, respectively. Similar time resolution was observed all across the area covered by the four pads, proving that a multipad detector can yield a time resolution comparable to a single-pad device.

6. – Conclusions

The progress towards a well understood, robust, large-area PICOSEC-Micromegas detector offering precise timing in the HL-LHC era and beyond was presented in this

work. Single-channel prototypes have demonstrated an excellent time resolution, of 76.0 ± 0.4 ps for timing a single photoelectron and 24.0 ± 0.3 ps for timing the arrival of a MIP, using a CsI photocathode which yields on average 10.4 ± 0.4 photoelectrons per MIP. The PICOSEC-Micromegas timing characteristics have been extensively studied in terms of detailed simulations and understood in detail in terms of a phenomenological model. Working towards a robust device, tests with resistive anode configurations were preformed, demonstrating tolerance to high particle fluxes but a somewhat worse time resolution. Various photocathodes were also tested for their robustness against ion backflow and storage conditions, as well as their quantum efficiency with promising results. Last, a multi-pad PICOSEC-Micromegas device was constructed and tested in muon beam and preliminary results show that the timing resolution is better than about 30 ps all across the area covered by the device.

$* * *$

REFERENCES

[1] WHITE S., *Experimental challenges of the European Strategy for particle physics*, in *Proceedings of the International Conference on Calorimetry for the High Energy Frontier (CHEF 2013) Paris, France, 2013*, arXiv:1309.7985 [physics.ins-det].
[2] PAPAEVAGELOU T. *et al.*, *EPJ Web of Conferences*, **174** (2018) 02002.
[3] BORTFELDT J. *et al.*, *Nucl. Instrum. Methods A*, **903** (2018) 317.
[4] GIOMATARIS Y. *et al.*, *Nucl. Instrum. Methods A*, **376** (1996) 29.
[5] GIOMATARIS I. *et al.*, *Nucl. Instrum. Methods A*, **560** (2006) 405.
[6] SCHNEIDER H. and VEENHOF R., *Garfield++ simulation of tracking detectors*, https://gar_eldpp.web.cern.ch/gar_eldpp/.
[7] PARASCHOU K., *Study of the PICOSEC Micromegas Detector with Test Beam Data and Phenomenological Modelling of its Response*, Master's Thesis, School of Physics, Aristotle University of Thessaloniki (2018) https://ikee.lib.auth.gr/record/297707/.
[8] BORTFELDT J. *et al.*, *Modeling the Timing Characteristics of the PICOSEC Micromegas Detector*, arXiv:1901.10779v1 [physics.ins-det] (2018).
[9] SOHL L. *et al.*, *J. Phys.: Conf. Ser.*, **1312** (2019) 012012.